Molecular Crystals and Liquid Crystals
Publication details, including instructions for authors and subscription information:
http://www.tandfonline.com/loi/gmcl16

A New Optical Phenomenon: Exciton Surface Polaritons at Room Temperature

M. R. Philpott [a], A. Brillante [a], I. R. Pockrand [a] & J. D. Swalen [a]
[a] IBM, Research Laboratory, San José, California, 95193, U.S.A.
Version of record first published: 21 Mar 2007.

To cite this article: M. R. Philpott , A. Brillante , I. R. Pockrand & J. D. Swalen (1979): A New Optical Phenomenon: Exciton Surface Polaritons at Room Temperature, Molecular Crystals and Liquid Crystals, 50:1, 139-162

To link to this article: http://dx.doi.org/10.1080/15421407908084422

Mol. Cryst. Liq. Cryst., 1979, Vol. 50, pp. 139–162

Printed in Holland

A New Optical Phenomenon:

Exciton Surface Polaritons at Room Temperature

M. R. PHILPOTT, A. BRILLANTE,† I. R. POCKRAND,† and J. D. SWALEN

IBM, Research Laboratory, San José, California 95193, U.S.A.

(*Received July 1, 1978*)

Exciton surface polaritons (ESP's) have been detected by attenuated total reflection spectroscopy on three organic solids at room temperature. This is the first time that ESP's have been observed *at room temperature on any material.* The three solids are: CTIP for γ-cyclopropyl-bis(1,3,3-trimethyl-indolenine-2-yl) pentamethinium fluoroborate, PTS for poly-2,4-hexadiyne-1,6-diol bis(p-toluene sulphonate) and TCNQ° for tetracyanoquinodimethane. These three materials are chemically very different, the first being an ionic crystal, and second a crystal of macroscopically long polymers, and the third a molecular crystal. The common property that allows all three to support ESP's is the existence of electronic transitions of very high intensity. These transitions have very wide polariton stop-bands within which one component of the dielectric tensor assumes negative values. This is a necessary condition for the existence of the surface polaritons.

1 INTRODUCTION

The phenomenon known as metallic reflection from molecular crystals was first seriously studied by Anex and Simpson[1] some twenty years ago. Since this pioneering work many organic crystals have been discovered that are insulators but which look like metals, that is, they have faces that reflect visible light well enough to give the crystals a metallic lustre. High reflectivity implies a frequency range within which the components of the dielectric tensor responsible for the effect go negative. These materials are therefore prime candidates in a search for insulators that will support at optical frequencies and at room temperature surface electromagnetic (EM) waves that are the counterparts of plasmon surface polaritons of real metals. Since it is a transition to a molecular exciton state that gives rise to the wide reflection

† IBM World Trade Postdoctoral Fellow 1977–1978.

bands, these surface EM waves are called exciton surface polaritons (ESP's). To date exciton surface polaritons (ESP's) have been observed only at temperatures of 77 K or less, on five inorganic solids (ZnO,[2] CuBr,[3] CuCl,[4] ZnSe,[5] CdS[6]) and one organic solid (anthracene[7]).

Exciton surface polaritons and plasmon surface polaritons are specific examples of a general class of surface wave called surface polaritons. Surface polaritons are electromagnetic waves coupled to the surface by electric (or magnetic) polarization fields and as such as macroscopic phenomena describable by Maxwell's equations. They have been studied extensively in the infrared and visible wavelength regions on inorganic semiconductors, ionic crystals and metals. Different types of electric (or magnetic) polarizations exist which give rise to different, though related, surface polaritons (SP's). Dielectric polarization caused by optical phonons can generate phonon surface polaritons and the oscillations of electrons at a metallic surface can produce plasmon surface polaritons. In insulators electronic transitions to exciton states are a source of polarization that can under certain conditions give rise to exciton surface polaritons (ESP's). The characteristic features of surface polaritons are:

1) their electromagnetic fields decay exponentially in directions perpendicular to the planar interface on which they propagate;

2) their electric field is *p*-polarized so that the E vector lies in the plane containing the surface normal and the direction of propagation, i.e., the sagittal plane (this is the same as the plane of incidence when SP's are excited by attenuated total reflection using a prism coupler); and

3) they exist in frequency ranges where the real part of the dielectric function is negative, as inside certain exciton bands of some crystals.

In this paper we will first briefly review the theory of ESP's and then describe the observation of exciton surface polaritons (ESP's) on surfaces of some highly reflecting organic solids at room temperature.[8,9] The purpose of the review is to provide some theoretical background for readers unfamiliar with this relatively new subject. At the end of the review, Section II, existence criteria are derived for metallic reflection and ESP's. These criteria are derived by a simple geometrical argument that has not been published elsewhere. The three organic solids are: CTIP for the cationic cyanine dye γ-cyclopropyl-bis(1,3,3-trimethylindolenine-2-yl) pentamethinium tetrafluoroborate, PTS for the polymerized diacetylene poly-2,4-hexadiyne-1,6-diol bis(p-toluene sulphonate), and TCNQ° for the neutral molecule tetracyanoquinodimethane. Figure 1 shows the schematic chemical structures of these organic materials. It will be shown that ESP's have a wide occurrence on organic materials, and for crystals displaying metallic reflection[1] are detectable at room temperature. In all observations reported to date, temperature

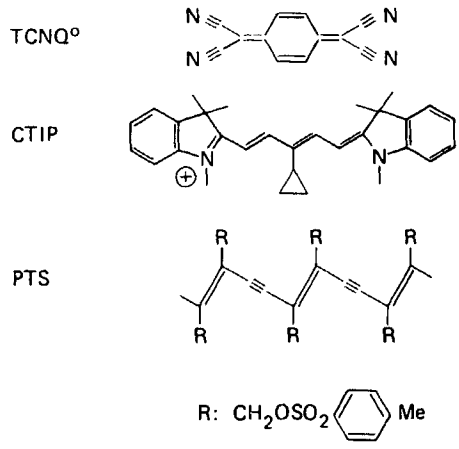

FIGURE 1 Schematic chemical structures of three organic materials shown to support exciton surface polaritons on crystals at room temperature.

of 77 K or less were needed, so that the presence of ESP's on these organics at room temperature makes the phenomenon almost as easy to study experimentally as phonon surface polaritons in the infrared or plasmon surface polaritons in the visible.

There is already a large literature on surface polariton phenomena and following the generally accepted convention we shall use the name "surface polariton" to describe all electromagnetic waves which are confined to a surface by electric or magnetic polarization. It was shown in the work of Cohen, Uller, Zenneck and Sommerfield[10] that electromagnetic waves can propagate along an interface between media, provided certain physical conditions hold. In the case where the two media are homogeneous, isotropic, non-magnetic, loss-free and separated by a planar interface; the necessary and sufficient condition is that $\varepsilon_a(\omega) + \varepsilon_b(\omega) < 0$, where $\varepsilon_a(\omega)$ and $\varepsilon_b(\omega)$ are the real dielectric functions of the two media.

In the limit that the discrete atomic or molecular structure of solids is neglected the properties of ESP's are obtained by solving Maxwell's equations with the solids treated as a polarizable continuous media. All that is required is a complete knowledge of the frequency (ω) and wavevector ($\vec{k}$) dependence of the dielectric permittivity and magnetic permeability tensors. However, at the microscopic level all three classes of surface polariton phenomena differ because the physical mechanism producing the electric polarization differs in each case. In passing we point out that the study of ESP's on organic solids is of great theoretical interest because it is possible to invent realistic microscopic theoretical models of surface polaritons on molecular crystals that are exactly solvable.[10] This has not

been possible for surface polaritons on metals where the elementary excitation is a plasmon or on inorganic insulators where the excitation is a Wannier-Mott exciton.

2 THEORY

Organic solids are often highly anisotropic, and the conditions under which ESP's occur are more complicated than those describing surface polaritons in isotropic solids. In order to give the reader a full appreciation of the experiments and their interpretation and some simple physical insights into surface polariton phenomena, we shall review briefly the theory of ESP's on isotropic and anisotropic solids in which there is no damping, the dielectric tensor being real. This also serves as an introduction to the concept of Brewster modes and various types of classifications of surface modes used in the literature.

The dispersion relation for ESP's on an isotropic surface active medium with a dielectric function $\varepsilon_b(\omega)$ is given by[11]

$$(c\kappa/\omega)^2 = \varepsilon_a \varepsilon_b(\omega)/[\varepsilon_a + \varepsilon_b(\omega)], \tag{1}$$

where κ is the wavevector, parallel to the surface plane and ε_a is the real dielectric constant of the surface inactive medium. This relation describes not only surface polaritons but also the Brewster modes, which are *p*-polarized waves impinging on the surface at the angle for which there is no reflected component. It is a simple matter to show that the Brewster angle condition

$$\tan\theta_B = \sqrt{\frac{\varepsilon_b}{\varepsilon_a}} \tag{2}$$

can be converted into Equation (1) by using the relations

$$\kappa = \frac{\omega}{c}\sqrt{\varepsilon_a}\sin\theta_B,$$

and

$$\sin^2\theta = \tan^2\theta/(1 + \tan^2\theta).$$

Therefore, a solution of Eq. (1) for the κ dispersion of ω yields both Brewster and surface polariton modes.

For a solid with a single exciton resonance the dielectric function $\varepsilon_b(\omega)$ is

$$\varepsilon_b(\omega) = \varepsilon_\infty + \frac{\omega_T^2 f}{\omega_T^2 - \omega^2}. \tag{3}$$

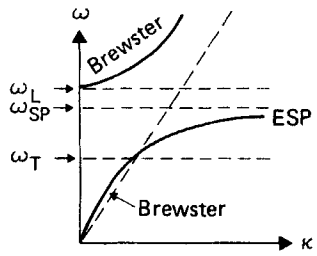

FIGURE 2 Schematic diagram of the dispersion curve (ω vs. κ) obtained by solving Equations (1) and (3). The relation between the longitudinal frequency, ω_L, and the transverse, ω_T, is given in Equation (5). The light line for air is shown as the sloping broken straight line.

Substitution of $\varepsilon_b(\omega)$ into the dispersion relation, Eq. (1), yields a quadratic equation for ω^2. The solutions of this equation are plotted schematically in Figure 2. The upper branch is a high frequency Brewster mode and the lower branch starting at $\kappa = 0$ describes a low frequency Brewster mode until the point $\kappa = \sqrt{\varepsilon_a}(\omega_T/c)$ is reached. At this point the mode becomes localized at the surface and crosses over to the surface polariton branch, labelled ESP in Figure 2. In the present context, since relaxation within the crystal has been assumed to be zero ($\gamma = 0$), the ESP's may also be correctly described as Fano modes, which are the ideal undamped surface electromagnetic waves. Also the SP mode has an asymptotic cut off given by

$$\omega_{SP}^2 = \omega_T^2[1 + f/(\varepsilon_a + \varepsilon_\infty)], \tag{4}$$

which shows that the ESP is frequency bounded and lies entirely within the polariton stop-band, i.e., $\omega_T \leq \omega \leq \omega_L$. Here ω_L is the longitudinal exciton frequency,

$$\omega_L^2 = \omega_T^2[1 + f/\varepsilon_\infty], \tag{5}$$

which is independent of the angle of incidence. There is no spatial dispersion since $\varepsilon(\omega)$ is independent of wavevector and no orientational dispersion of the exciton since the solid is isotropic.

It is characteristic of surface polaritons of all types that the cut-off frequency, ω_{SP}, which corresponds to the surface state frequency in the absence of retardation (limit $\kappa \to \infty$), depends on the dielectric constant of the surface inactive medium. The effect of increasing ε_a is to compress the frequency range of the surface mode, by pushing ω_{SP} closer to the transverse exciton frequency ω_T. Notice that the ESP dispersion lies on the right-hand side of the light-line of the surface inactive medium; photons incident on the crystal face now *cannot* excite the surface wave because it is not possible to simultaneously match frequency ω and surface wavevector κ. If, on the other hand, another inactive medium with refractive index $n_g > n_a$ (where $n_a = \sqrt{\varepsilon_a}$) is

brought close to the surface (but not close enough to significantly disturb the dispersion of the ESP), then it is possible to couple photons to the ESP. The coupling arises when the dispersion line of the prism photon intersects the ESP dispersion curve. In other words it is now possible to match frequency and wavevector of a prism photon to those of an ESP. This is the principle of detection of surface waves by attenuated total reflection (ATR) spectroscopy.

Surface polaritons with a dispersion given by Eq. (1) are defined for all values of the surface wavevector κ greater than the minimum value $\kappa_T = \omega_T n_a/c$. This is clear from the curve in Figure 2. These modes are called real surface polaritons because there is no volume polariton with a wavevector parallel to the surface which can match phase and frequency with this ESP. Put another way, volume polaritons are excluded from the frequency range $\omega_T < \omega < \omega_L$ because the stop-band is invariant under changes in the direction of the three dimensional wavevector, $\vec{k}$.

Organic solids are rarely isotropic and a more complex model is needed to describe ESP's on the surfaces of anisotropic crystals. The next step in complexity is to assume that the surface active medium is orthorhombic with the principal dielectric axes along the coordinate axes x, y and z where the unit vector $\hat{z}$ is perpendicular to the surface and points into the crystal. The wavevector κ of the surface wave is taken to be parallel to the $\hat{x}$ unit vector. It has been shown[13–15] that now the dispersion relation for ESP's polarized with an electric vector in the xz plane is

$$(c\kappa/\omega)^2 = \frac{\varepsilon_a \varepsilon_z(\varepsilon_a - \varepsilon_x)}{\varepsilon_a^2 - \varepsilon_x \varepsilon_z}. \tag{6}$$

This same relation also describes a Brewster mode which is for anisotropic solids the p-polarized mode for which the reflectivity R_p is zero. The Brewster angle is given by

$$\tan\theta_B = \left[\frac{\varepsilon_z(\varepsilon_a - \varepsilon_x)}{\varepsilon_a(\varepsilon_a - \varepsilon_z)}\right]^{1/2} \tag{7}$$

It is important to recall that excitons in orthorhombic crystals have properties different from those in isotropic solids, but that they are similar in many ways to those observed in crystals of the monoclinic class. For example, excitons with an $\vec{E}$ field in the xz plane exhibit orientational dispersion. The energy of this exciton (if the symmetry were uniaxial this exciton mode would be called the extraordinary mode) is[16]

$$\omega^2 = \omega_T^2 + \omega_T^2(\cos\phi)^2 f/\varepsilon_\infty, \tag{8}$$

where ϕ is the angle between the transition dipole and the wavevector. As the angle between the three dimensional wavevector and the transition moment changes, the energy of the coulombic exciton shifts from $\omega_T(\phi = \pi/2)$ to

$\omega_L(\phi = 0)$. If the third component ε_y has the form given by Equation (3), then this exciton at ω_{T_y} shows no orientation dispersion and in a uniaxial crystal would be referred to as an "ordinary" exciton.

Several cases of great practical interest are approximated by a model for which the dielectric component, ε_z, perpendicular to the crystal surface is effectively independent of frequency over a limited range, and the component, ε_x, parallel to the direction of propagation is given by Eq. (3). This geometry approximates the crystals selected for ESP experiments; namely the polymeric crystal, PTS; the cationic cyanine dye crystal, CTIP; and the neutral molecule crystal, TCNQ°, each for specific crystal faces.

It has been shown that there is no surface polariton solution if $0 < \varepsilon_z < \varepsilon_a$.[13-15] When $\varepsilon_z > \varepsilon_a$, there is a volume exciton-polariton mode with a wavevector parallel to the x-axis and an electric vector $\vec{E}$ parallel to the z axis, which intersects the ESP in the frequency range where $\varepsilon_x(\omega)$ is negative. The ESP branch ceases at the intersection point, connecting to a volume exciton polariton, and its range in wavevectors is bounded. Because this type of ESP is found only near the light line, it has been called a virtual ESP,[13-15] in contrast to the real ESP's of an isotropic crystal, which were discussed earlier. It is possible that organic crystals with real ESP could be found. The simplest case would be a crystal with two molecules per unit cell oriented in such a way that ε_x and ε_z have common frequency regions, where the dielectric components are both negative.

So far we have described the case of non-absorbing solids. In real solids, however, there are complicated frequency independent relaxation processes which reduce the reflectivity within the stop-band regions. The simplest way of including a damping process is to include a phenomenological term $-i\omega\gamma$ in the denominator of the expression for ε_b, Eq. (3), which becomes

$$\varepsilon_b(\omega) = \varepsilon_\infty + \frac{\omega_T^2 f}{\omega_T^2 - \omega^2 - i\omega\gamma}. \tag{9}$$

With the inclusion of ε_b in the form given by Eq. (9) the dispersion relations (1) and (6) become complex and it is necessary to define the experimental conditions by which the surface modes are to be excited. The two most commonly used experimental ATR configurations correspond to R_p vs. θ (ω constant) and R_p vs. ω (θ constant) which we shall, henceforth refer to as angle and frequency scans, respectively. The complex properties of ω and κ are different for each case and have been discussed fully (see Reference 10d). The important point is that there is no longer a sharp division between the Brewster mode and the surface polariton. Minima in the ATR spectra can occur on either side of θ_c, the critical angle, for the prism-air interface. In the case where $|Re\varepsilon(\omega)| \gg Im\varepsilon(\omega)$, the surface modes resemble those corresponding to $\gamma = 0$ in the theoretical models. These modes are often referred to as

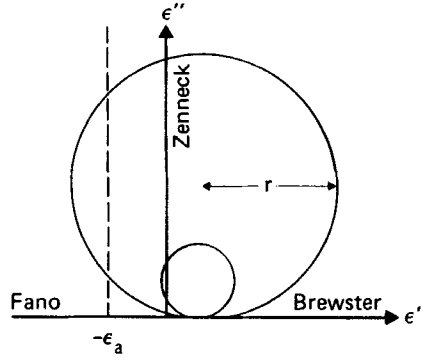

FIGURE 3 A schematic diagram of the imaginary part of $\varepsilon(\omega)$ plotted against the real part of $\varepsilon(\omega)$. The dielectric function $\varepsilon(\omega)$ is defined by Equation (9). The large circle is for small damping and the small circle is for large damping. The locations of the three limiting regions, Fano, Zenneck and Brewster, are shown. See the text for more details.

Fano modes. Surface modes also occur when $|Re\varepsilon(\omega)| \simeq Im\varepsilon(\omega)$ and these having no formal counterpart in the $\gamma = 0$ regime, are often referred to as Uller–Zenneck or more simply as Zenneck modes. Actually the same solid may support all types, there being a continuous blending from one to the others. This is shown in Figure 3, where we have plotted $Im\varepsilon(\omega)$ against $Re\varepsilon(\omega)$ for dielectric functions with the form of Eq. (9) corresponding to very different values of the damping parameter γ. The Fano region lies close to the real negative axis, the Zenneck region on the positive imaginary axis, and the Brewster region on the positive real axis. Organic solids tend to be more in the Zenneck region whereas metals, like silver, tend to be in the Fano region and lie close to the real axis for visible frequencies.

The dispersion relations (1) and (6), for isotropic and anisotropic crystals, respectively, can easily be solved for any values of the damping parameter γ, under the assumption that ω is real and κ is complex, as required for angle scan ATR experiments. Figure 4 plots of ω against the real part of κ for the anisotropic (virtual ESP) case. Three values of the damping have been selected that simulate the experimental dispersion curves of CTIP, PTS and TCNQ°. The parameters used were $\varepsilon_a = 1.0$, $\varepsilon_{\infty x} = \varepsilon_z = 2.25$ and $f = 1.0$.

Damping affects the real ESP more because for this mode both the x and z components of the EM field are coupled the dissipation process. In the case of both real and virtual ESP's the effect of increasing the damping is to pull the mode out of the nonradiative region where $c\kappa > \omega$, into the radiative region where $\omega > c\kappa$.

The simplest occurrence criterion for ESP's is the existence of metallic reflection[1] from the surface of the organic solid. If the solid displays metallic reflection then as noted in the introduction, there is a distinct possibility

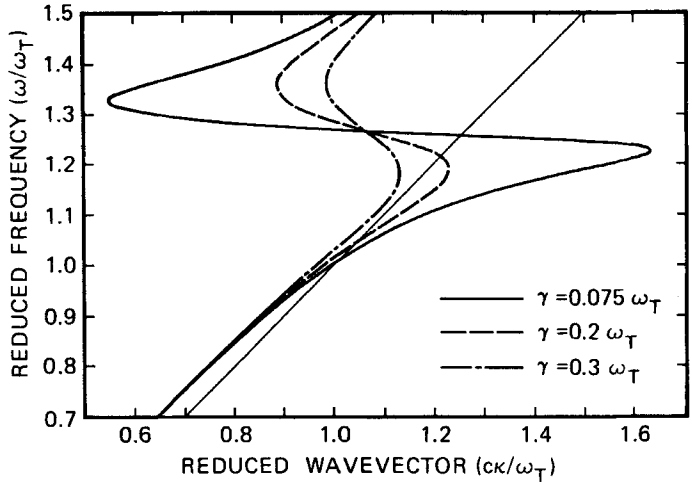

FIGURE 4 Effect of damping on the dispersion ω vs. Re κ of an ESP of an anisotropic crystal, showing the existence of back bending in the dispersion curve for three large values of the damping parameter γ. The parameters used in the calculation were $\varepsilon_a = 1$, $\varepsilon_{\infty x} = 2.25$, $\varepsilon_z = 2.25$, $f = 1.0$ and $\gamma = 0.075\ \omega_T$, $0.2\ \omega_T$, $0.3\ \omega_T$.

than ε'_x is less than -1 for frequencies corresponding to the metallic color. In the notation of Eq. (9) the condition for metallic reflection, as formulated by Anex and Simpson,[1] is

$$f > 2\varepsilon_\infty \gamma/\omega_T. \tag{10}$$

The damping or relaxation parameter γ is the reciprocal of the lifetime of the exciton in the solid. In applications of inequality (10) it is well to bear in mind that the systems for which it was proposed are organic dye stuffs. The electronic transitions of these materials display little or no vibronic structure and it was found empirically that within experimental error γ was equal to the half width of the transition in solution at low concentration. Typically $\gamma \simeq 3000\ \text{cm}^{-1}$, $\omega_T \simeq 20{,}000\ \text{cm}^{-1}$ and $\varepsilon_\infty \simeq 3$, which implies that the oscillator strength f should be greater than unity for metallic reflection to occur. An alternative way of writing criterion (10), involving the width of the polariton stop-band, is

$$\Delta\omega = \omega_L - \omega_T > \gamma. \tag{11}$$

Since $\Delta\omega$ is also a measure of the coulombic exciton band width, this last relation is the solid state equivalent of the criterion for strong vibronic coupling in dimers as put forward by Simpson and Peterson.[17]

The criterion expressed by inequality (10) does not take into account the requirement that $\varepsilon'(\omega) < -\varepsilon_a$ for nonradiative surface waves on an isotropic

solid. In a sense (10) is a necessary but not sufficient condition. To derive a necessary condition a simple geometrical argument suffices.

It is a simple matter to show that the locus of $\varepsilon''(\omega)$ against $\varepsilon'(\omega)$, as shown in Figure 3, for example, is approximately an open circle centred at $(\varepsilon_\infty, \frac{1}{2}\varepsilon''(\omega_T))$. The locus has a segment missing between the points $\varepsilon' = \varepsilon_\infty$ and $\varepsilon' = \varepsilon(0)$ on the real axis. The radius of the circle is $\frac{1}{2}\varepsilon''(\omega_T)$ or equivalently $\frac{1}{2}(\omega_T f/\gamma)$. The geometric interpretation of inequality (10) is now evident, it is simply a statement that all circles with radii greater than ε_∞ cut the vertical ε'' axis. In other words for a crystal to show metallic reflection the plot ε'' vs. ε' must touch or cut the ε'' axis. By analogy the necessary condition for the existence of real ESP's is

$$f > 2(\varepsilon_\infty + \varepsilon_a)\gamma/\omega_T. \tag{12}$$

Geometrically this corresponds to circles ε'' vs. ε' that touch or cut the line $\varepsilon' = -\varepsilon_a$.

3 EXPERIMENTAL RESULTS

The method of ATR used in the experiments is shown schematically in Figure 5. A crucial problem encountered in these experiments is the setting of the air gap between the prism and the crystal, to the wavelength of the incident light. Even with the best faces the gap varied widely over the width of the laser beam, due to irregularity of the sample. To reduce this problem we focused the laser beams to a small spot.[18] This was accomplished by first expanding a *p*-polarized beam with an inverted telescope and spatial filter

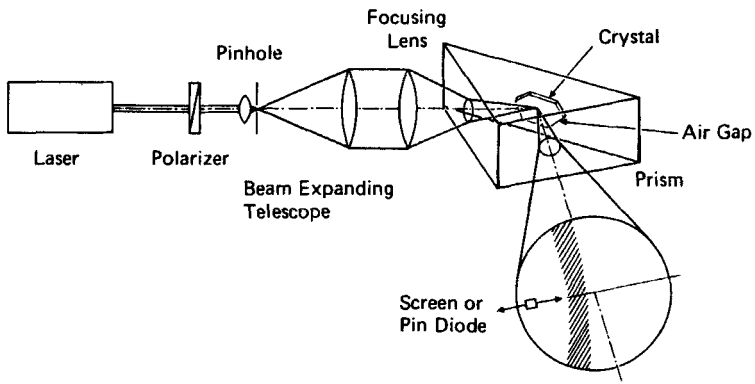

FIGURE 5 Schematic diagram of the focused beam method of making ATR angle scans of crystals with irregular surfaces.

to a width of 40 mm and subsequently focusing the expanded beam onto the base of the prism using an achromatic wide angle lens (focal length = 28 mm). The prism faces were optically flat to within $\lambda/10$. For spot sizes smaller than the irregularities in a particular region of the crystal surface the prism-crystal separation was uniform. Regions suitable for the ATR experiment were found by translating the spot across the base of the prism. The gap between the crystal and prism was changed by adjusting the pressure applied to the prism. Once a suitable position on the crystal was located and an optimum gap obtained, the ATR spectrum was measured by moving a pin diode detector through the cone of light reflected from the prism. By changing the wavelength from 632.8 to 441.8 nm, we were able to determine the dispersion of the surface modes throughout the region of the stop-bands. At the end of a sequence of experiments the prism was translated and the total internal reflection spectrum for the prism-air interface was measured to set the angular and reflectivity scales. As already mentioned the air gap was adjusted at each wavelength in order to optimize the coupling to the surface polariton.

3.1 ATR Spectra of CTIP

Crystals of CTIP were grown from a hot saturated methanol solution that was allowed to cool slowly over a period of several days. The crystals grew as large 5 × 4 × 2 mm prismatic shapes with well developed silver coloured (110) and (010) faces and blue coloured (100) faces. Some samples had (110) faces with dimensions as large as 5 × 4 mm, though they were rarely flat over areas this large. The experiments reported here were performed on the (110) face, experiments have also been performed on the (010) and (100) faces. In passing we note that silver metallic reflection from organic materials is virtually unknown, only $(CH)_x$, its derivatives[19,20] and CTIP[21,22] display reflectivity high enough over all visible frequencies to show this phenomenon.

The crystal structure of CTIP is triclinic $P\bar{1}$ with two molecules per unit cell. The cations are parallel and packed approximately in the (112) plane.[23] It is entirely reasonable to assume that the transition dipole lies along the chain axis so that in the crystal the transition polarized along the chain axis is allowed and that perpendicular is forbidden. Also since the electronic transition is well removed from all others it should be entirely responsible for the anomalous dispersion of the dielectric tensor. Consequently the optical properties of the crystal are equivalent to those of an orthorhombic solid with one principal axis parallel to the chain axis and the other two perpendicular to the chain axis. Furthermore since the chain axis is inclined at an angle of only 9.4° to the (110) plane, as a first approximation one can assume that the dielectric tensor is diagonal in the $\hat{x}$, $\hat{y}$, $\hat{z}$ coordinate system of Eq. (1).

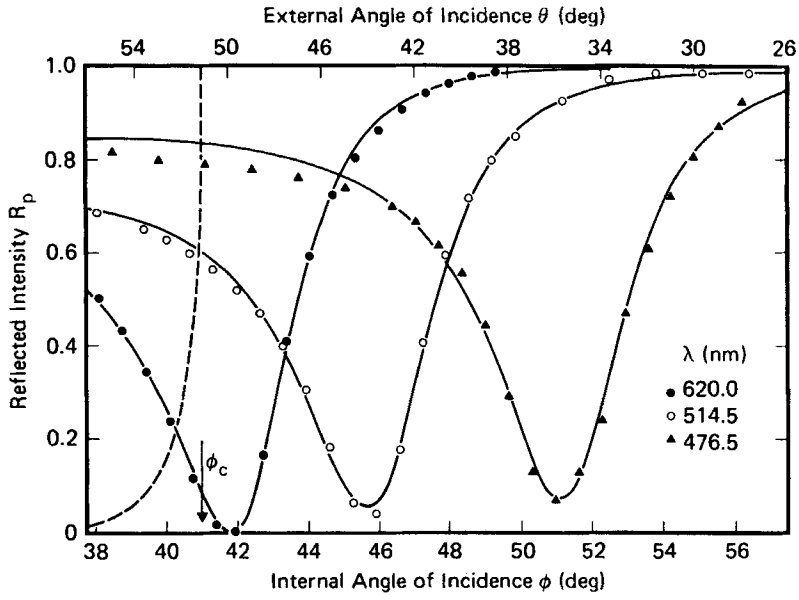

FIGURE 6 ATR *p*-polarized spectra of CTIP face (110) for three wavelengths. At 620 nm the gap is 397 nm and $\varepsilon_x = -9.10 + i6.61$; at 514.5 nm the gap is 278 nm and $\varepsilon_x = -2.62 + i0.95$; at 476.5 nm the gap is 206 nm and $\varepsilon_x = -1.14 + i0.23$ for the theoretical solid curves. In all cases the dielectric function normal to the (110) face was assumed to be $\varepsilon_z = 2.6$. The dashed line shows the reflectivity from the air-prism interface and the limiting value is marked for the critical angle ϕ_c.

The exciton band therefore has two branches, one with a strongly allowed transition parallel to the polymethinium chains and the other polarized perpendicularly to the chains with vanishingly small intensity. Of course second order interactions can give this second branch some intensity but as examinations of the reflection spectrum at room and at 2°K show no sharp structure; it is, therefore, reasonable to neglect this second branch as a good first approximation.

Figure 6 shows a representative set of *p*-polarized ATR spectra of the (110) face of CTIP. The data points are measured values and the curves were obtained by fitting Fresnel's formula of the layered system to the experimental results. The dashed curve gives the internal total reflectivity spectrum of the prism-air system without the crystal being present. Note that all resonance minima are located to the right of the critical angle ϕ_c in the non-radiative region ($\phi > \phi_c$), which is a characteristic property for surface polaritons.

In Figure 7 the experimentally determined dispersion of the exciton surface polariton is shown in a plot of wavelength and energy of the exciting light

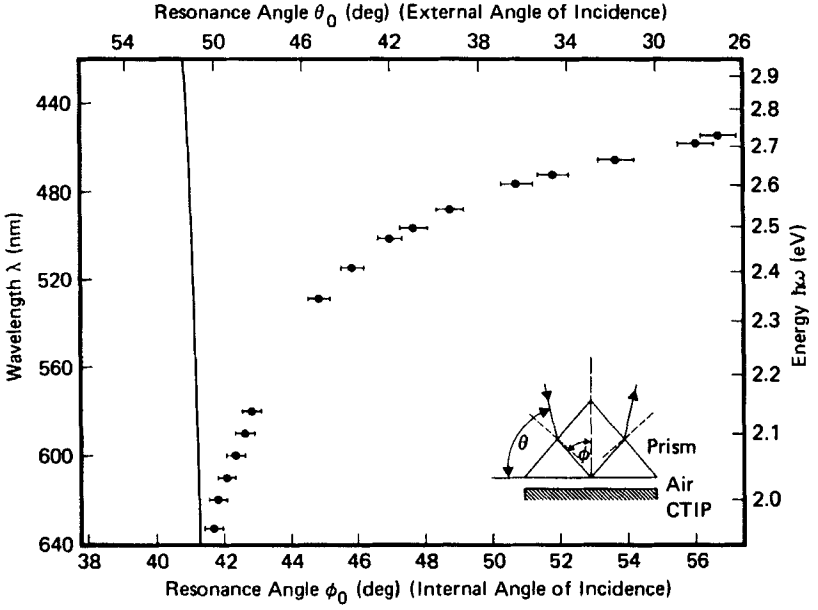

FIGURE 7 Experimental dispersion curve of wavelength in nm and energy in eV as a function of internal and external angles of incidence. The almost vertical line is the critical angle, i.e., the light line. A lower right inset shows the experimental configuration.

versus the angle of the reflection minimum (internal and external resonance angle ϕ_0 and θ_0, respectively). The wavevector of the ESP is $k_x = (\omega/c) \cdot n_p \cdot \sin\phi_0$, where n_p is the refractive index of the prism. The negative slope of the light line in Figure 7 ($\phi_0 = \arcsin(1/n_p)$) is due to the change in the prism refractive index with wavelength. We measured a difference of up to 18 degrees between the light line and the ESP resonance, an indication of considerable dispersion. The air gap in the experiments had to be adjusted for different spectral regions because of the large variation of the dielectric function of CTIP in the wavelength region investigated. Therefore the dispersion curve given in Figure 10 was obtained from measurements with slightly different gap widths.

The experimental ATR spectra were analysed to calculate the dielectric function $\varepsilon_x = \varepsilon_x' + i\varepsilon_x''$ and gap distance d assuming that $\varepsilon_z = 2.6$ was constant, independent of frequency. This value of ε_z is the same as the background value of the dielectric component ε_x. The values of ε_x determined (see caption Figure 6) were used to obtain the spatial dependence of the electromagnetic field intensity of the ESP's shown in Figure 8, where $\frac{1}{2}|\vec{H}|^2$ is plotted as a function of z across the layered system consisting of prism air gap and crystal. The p-polarized intensity, calculated for the resonance angle

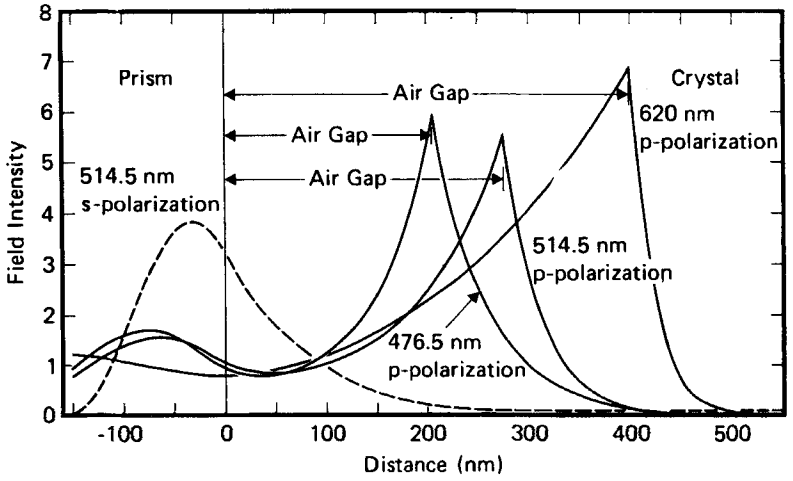

FIGURE 8 The electromagnetic field intensity $\frac{1}{2}|\vec{H}|^2$ as a function of distance along the z-axis through the prism–air–crystal structure for the wavelengths 620 nm, 514.5 nm and 476.5 nm. Each curve was calculated at the internal resonance angle ϕ_0, using the same parameters as in Figure 6. Note that because the experimental gap varied for each reflectivity curve given in Figure 6, the crystal surface appears at different z values.

ϕ_0 of the curves of Figure 6, shows the behavior typical for the excitation of a surface wave, namely a resonantly enhanced field intensity at the air-crystal interface. For CTIP this effect is more pronounced for the long wavelength. In contrast the s-polarized intensity, where no surface polaritons are excited, shows only the character of an evanescent field.

The remarkable feature of Figure 7 is the fact that the ESP was not observed at all in the radiative region, which lies to the left of the light line (solid line). Referring back to Figure 4 we see that the type of dispersion exhibited is qualitatively similar to the $\gamma = 0.075\,\omega_T$ curve. We shall see that the ESP's on PTS and TCNQ° resemble the other two curves in Figure 4, so that a rather complete range of examples have been studied in our experiments.

3.2 ATR Spectra of PTS

At room temperature PTS is a monoclinic crystal with space group $P2_1/c$, having two zig-zag polymer chains passing through a unit cell, each parallel to the unique monoclinic b axis.[24] The plane of the zig-zag is not parallel to the main cleavage face (100) but inclined at an angle of 17°. The optical properties of PTS have been determined at room temperature and at low temperature by reflection spectroscopy.[25–27] There is some evidence that the electronic transition dipole of a single chain is not directed exactly along the

chain axis but is inclined to it at an angle of approximately 14° within the plane of the zig-zag chain.[28,29] The crystal should, therefore, display two allowed volume exciton transitions, one parallel to the b axis and the other perpendicular to it. The projection of the transition dipole moment on the perpendicular direction is, however, much smaller than the projection on the parallel direction. Furthermore, this perpendicular projection has only a small $\hat{z}$ component (unit vector $\hat{z}$ is normal to the (100) crystal face). Therefore in the present analysis we shall ignore the weak $\hat{z}$ component of the perpendicular transition and treat the optical properties as if the crystal were orthorhombic with the b axis parallel to the $\hat{x}$ direction.

In our experiments monomer crystals of 2,4-hexadiyne-1,6-diol bis (p-toluene sulphonate) were grown from methanol solution by slow evaporation at room temperature. These monomer crystals were cleaved parallel to the (100) face. An important physical property of these and related diacetylene crystals is the ease with which the basal face may be cleaved to give relatively large areas free of visible imperfections. This property is crucial for ATR experiments because the air gap between the prism and the crystal must be set to the order of the wavelength of the light used. The monomer crystals were polymerized in the dark at a temperature of 60°C under vacuum. The procedure of cleavage before polymerization yields better surfaces because the cleaved polymer crystals often have faces spoiled by the presence of loosely attached polymer fibrils.

Figure 9 shows the ATR curves for a PTS crystal at 295°K as a function of the angle of incidence for three different wavelengths, 600, 610 and 620 nm. The experimental points coincide in each case almost exactly with the theoretical curve derived from a least squares computer fit to Fresnel's equations. The theoretical parameters used in the calculation are given in the caption to Figure 9. The fourth solid curve from $R_p = 0$ to $R_p = 1$ at the critical angle, ϕ_c, is the internal reflection of the prism-air interface where there was no crystal. As in the case of CTIP this curve was used to set the angular and reflectivity scales for the ATR measurements. Figure 10 shows the dispersion (λ vs. the internal angle, ϕ, and also the external angle to the prism base, θ) of the ESP's determined by plotting the wavelength versus the angular position of the reflectivity minimum.

Starting at $\lambda = 632.8$ nm in the radiative region the dispersion curve, shown in Figure 10, crosses the light line at $\lambda \simeq 607$ nm, into the non-radiative region where $c\kappa$ is greater than ω. It then bends back and returns to the radiative region where $c\kappa$ is less than ω. This behavior resembles the $\gamma = 0.2\,\omega_T$ curve in Figure 4.

Returning to Figure 10 we can now describe the evolution of the ESP along the dispersion curve. At the longest wavelength the ESP can be described as a damped Brewster mode. In the region of crossing the light line the damping

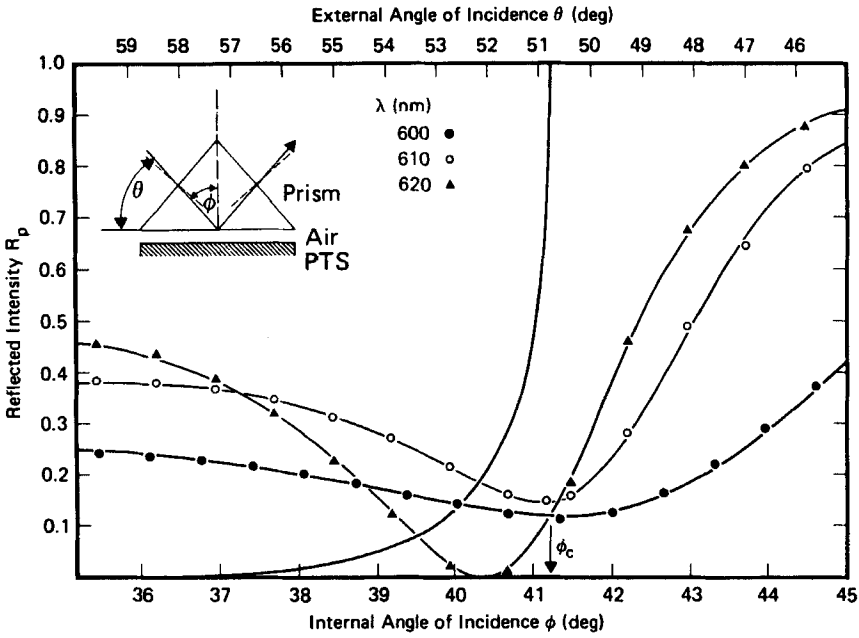

FIGURE 9 Reflectivity intensity R_p as a function of angle, internal angle (ϕ) on the lower abscissa and external prism angle (θ) on the upper abscissa, for three wavelengths. At 600 nm the gap is 319 nm and $\varepsilon_x = -1.11 + i3.92$; at 610 nm the gap is 488 nm and $\varepsilon_x = -3.19 + i8.65$; and at 620 nm the gap is 530 nm and $\varepsilon_x = 2.78 + i22.22$ for the theoretical solid curves. In all cases the dielectric function normal to the (100) face was assumed to be $\varepsilon_z = 2.48 + i0.003$. The reflectivity from the air-prism interface is shown as the fourth curve and the limiting value is marked for the critical angle, ϕ_c. An upper left inset schematically shows the experimental configuration.

is very heavy and the ESP is a Zenneck or a very lossy Fano mode. At slightly shorter wavelengths the surface polariton crosses back into the radiative region on the left side of the light line and once again becomes a Brewster mode. At room temperature the ESP on PTS does not penetrate very far into the nonradiative region.

In Figure 11 the relative electromagnetic intensity is shown as a function of the z position across the layered structure, prism-air gas-crystal, at the minimum reflectivity angles for the three curves of Figure 9. Notice how the intensity peaks at the crystal surface and decays away from the interface very rapidly for each case. This enhancement of the field intensity at the crystal surface is a distinctive characteristic of surface waves. Also shown in the Figure 9 is the intensity of the s-polarized wave which exhibits the decay curve typical of an evanescent field created by total internal reflection. Notice that the ratio of the peak field intensity on the crystal surface to that within the prism is smaller for PTS than for CTIP, reflecting the fact that in CTIP the ESP is more localized.

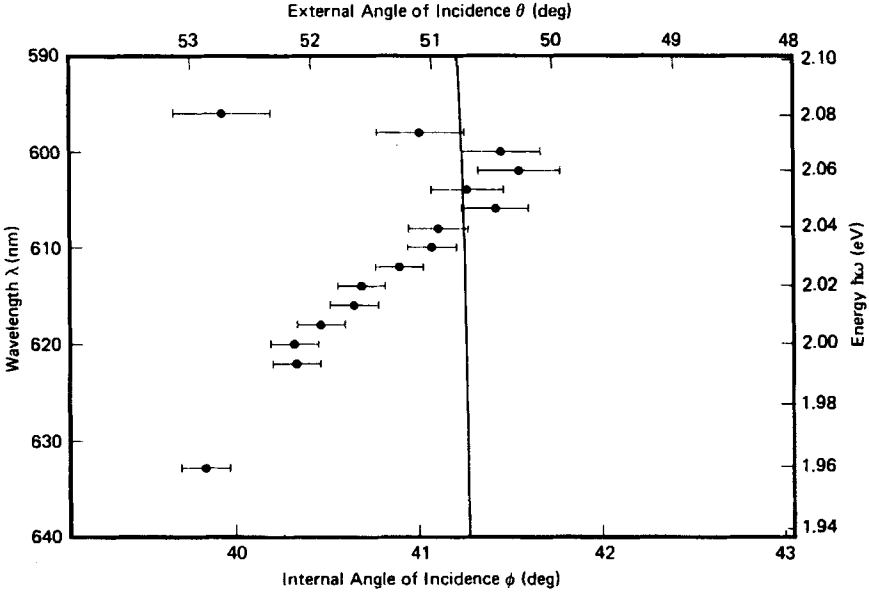

FIGURE 10 Experimental dispersion curve of wavelength in nm and energy in eV as a function of internal and external angles. (See the inset in Figure 9 for the definition of the angles.) The almost vertical line is the critical angle, i.e., the light line.

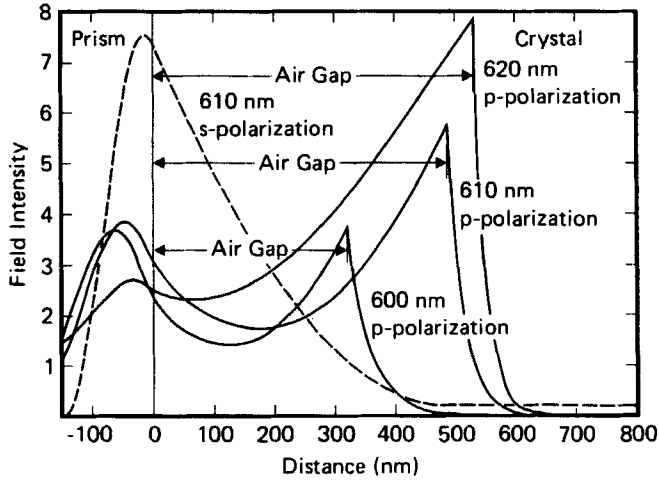

FIGURE 11 The electromagnetic field intensity $\frac{1}{2}|\vec{H}|^2$ as a function of distance along the z axis through the prism–air gap–crystal structure for the wavelengths: 600, 610 and 620 nm. Each curve was calculated at the reflectivity minimum of the ATR spectra, but because the experimental gap varied for each reflectivity curve given in Figure 9 the crystal surface appears at a different z value.

3.3 ATR Spectra of TCNQ°

Crystals of TCNQ° were grown from a hot saturated acetonitrile solution that was allowed to cool slowly over a period of several days. The crystals grew as large as 10 × 10 × 3 mm parallelopipeds with well developed (001), and (110) faces and small blue (010) faces. The TCNQ° had previously been purified by vacuum sublimation and recrystallization. The acetonitrile was purified by distillation over pure TCNQ°.

At room temperature the TCNQ° crystal has space group $C2_1/c$ and the unit cell with parameters $a = 8.906$ Å, $b = 7.060$ Å, $b = 16.395$ Å, $\beta = 98.54°$ contains four molecules.[30] The visible singlet electronic transition of the molecule is polarized along the long in-plane axis of the molecule ($^1B_{3u} \leftarrow {}^1A_{1g}$) and is very intense, the oscillator strength of the transition in solution being greater than 0.9.[31] In the crystal this intense molecular transition gives rise to a very wide exciton band extending from 2.8 eV to 4.3 eV. There are two allowed exciton transitions, one very intense one polarized perpendicularly to the unique monoclinic b axis and the other relatively weak polarized parallel to the crystallographic b axis. For the (010) face the polariton stop-band of the $\perp b$ transition, which spans the range 2.8 eV to 4.3 eV, is responsible for the blue metallic color of this face. This means, of course, that the energy range of the ESP is large.

Figure 12 shows the ATR curves for the (010) face of a TCNQ° crystal at 295°K as a function of the angle of incidence for three different wavelengths,

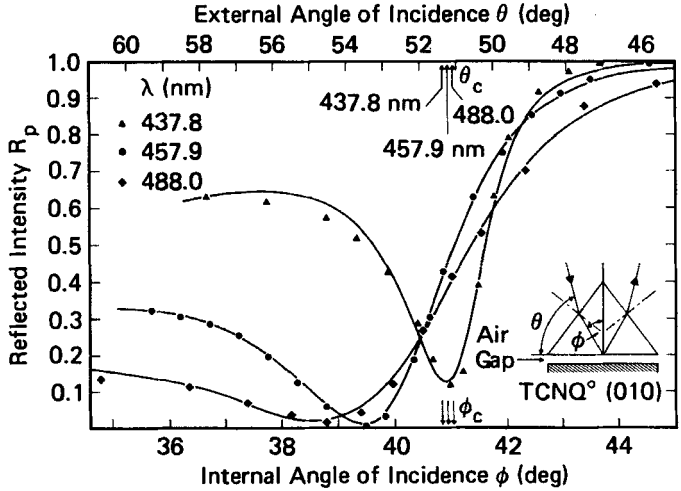

FIGURE 12 ATR p-polarized spectra of TCNQ° face (010) for three wavelengths. At 488 nm the gap is 405 nm and $\varepsilon_x = 11.63 + i5.17$ with $\varepsilon_z = 2.46 + i0.11$; at 457.9 nm the gap is 441 nm and $\varepsilon_x = 28.03 + i15.13$ with $\varepsilon_z = 2.65 + i0.21$; at 437.8 nm the gap is 514 nm and $\varepsilon_x = -18.05 + i16.8$ with $\varepsilon_z = 2.64 + i0.56$.

488, 457.9, and 437.8 nm. The data points are the measured values and the theoretical curves were obtained by a least squares computer fit to Fresnel's equations for a three layered system. The third layer, representing the crystal, was assumed to be biaxial with principal directions coincident with the axes used in Eq. (1). In deriving these results the complex component ε_z was assigned the values calculated by Pennelly and Eckhardt[31] by a Kramers–Kronig transformation of the (010) reflectivity spectrum. The computer fits yielded complex ε_x and the width of the air-gap. These parameters are given in the caption to Figure 12.

In Figure 13 the experimentally determined dispersion of the exciton surface polariton is shown in a plot of wavelength and energy of the exciting light versus the angle of the reflection minimum (internal and external resonance angle ϕ_0 and θ_0, respectively). Starting at $\lambda = 515$ nm in the radiative region the dispersion curve, shown in Figure 13, crosses the light line at $\lambda \simeq 442$ nm, into the nonradiative region where $c\kappa$ is greater than ω. It then bends back and returns to the radiative region where $c\kappa$ is less than ω. This behavior is more extreme than that observed for PTS and resembles the dispersion of the most heavily damped curve, with $\gamma = 0.3\,\omega_T$, in Figure 4. We

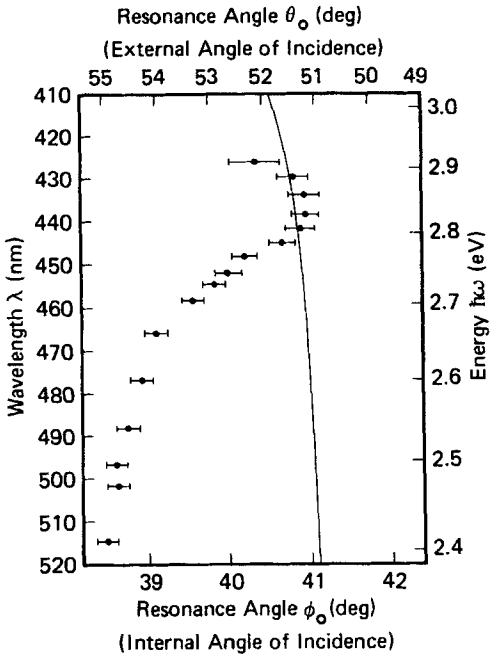

FIGURE 13. Experimental dispersion curve of wavelength in nm and energy in eV of the ATR minimum of TCNQ° as a function of internal (ϕ_0) and external (θ_0) angles.

note that the ESP only just enters the nonradiative region, in spite of a very large negative ε_x' in the spectral range studied ($\lambda \simeq 440$ nm). At liquid helium temperatures the excursion past the light line is expected to be much larger, and more structure is expected in the dispersion curve because of the presence of strong intramolecular phonons.[32]

In Figure 14 the relative electromagnetic field intensity is shown as a function of the z position across the layered structure, prism-air gap-crystal. The p-polarized intensity, calculated for the resonance angle ϕ_0 of the curves of Figure 14, and the same gap and dielectric parameters shows the behavior typical for the excitation of a surface wave, namely a resonantly enhanced field intensity at the air-crystal interface. For the (010) face of TCNQ° this effect is more pronounced for the short wavelength. As in earlier examples the s-polarized intensity, where no surface polaritons are excited, shows only the character of an evanescent field.

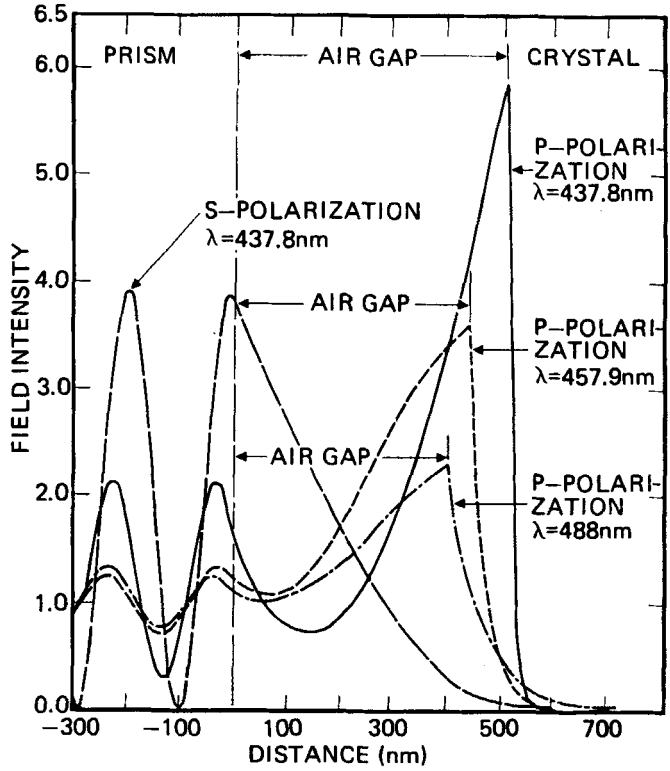

FIGURE 14 The electromagnetic field intensity ($\frac{1}{2}|\vec{H}|^2$) as a function of distance along the z axis through the prism–air gap–crystal, for the wavelengths: 488 nm, 457.9 nm and 437.8 nm. The air gap and angle of incidence are for each of the three wavelengths the same as those given in the caption to Figure 12.

4 DISCUSSION

It was mentioned in the introduction that as a class surface polaritons have the following general characteristics: (i) the electromagnetic field decays exponentially in directions perpendicular to the surface; (ii) the $\vec{E}$-field is polarized in the sagittal plane; (iii) they exist in frequency ranges where the real part of the dielectric function is negative. The last characteristic needs some qualification because it applies strictly only when there are no absorption processes. In the absence of absorption there is a clear distinction between Brewster modes and surface waves since the former are not bound to the surface and extend to infinity in directions perpendicular to the surface. However, if absorption occurs at a given frequency the amplitude of the Brewster mode can decay exponentially with distance from the surface and therefore has the first two characteristics listed above. Furthermore, as the experiments for CTIP, PTS and TCNQ° have shown there is no fundamental change in the shape of the ATR minimum as λ changes and as θ_{ESP} moves past the critical angle θ_c; there is therefore no operational basis for distinguishing "damped" Brewster modes from surface polaritons. Accordingly we use the term surface polariton henceforth to describe Brewster, Zenneck and Fano modes.

We are now in a better position to compare ESP's on CTIP, TCNQ° and PTS. It is clear from the optical data of Weiser, *et al.*[21,22] that CTIP has frequency regions where the magnitude of ε_x' is up to four times greater than ε_x''. Accordingly the ESP lies in the Zenneck region and may even be described as a lossy Fano mode. Figure 6 shows several ATR minimum lying on the right of the critical angle in the nonradiative region the furthest point being almost eighteen degrees past the critical angle. The theoretical calculations of Figure 8 show that there is a resonance in the field intensity at the crystal surface almost an order of magnitude greater than the field in the prism. This resonance is not as great as for metallic silver where several orders of magnitude change occur, but nevertheless the enhancement in field intensity is large. Further experiments are needed with prisms of higher refractive index and at wavelengths shorter than 460 nm to look for back bending in the dispersion curve as well as the effects of coupling to the bulk polaritons which should damp out the ESP.[33]

In contrast the ESP on PTS never moves much beyond the light line when $\varepsilon_x' < 0$, and consequently is best described in the nonradiative region as a Zenneck mode. Figure 9 illustrates well the difficulty, discussed above, of separating damped Brewster modes from surface polariton waves. The ESP never evolves beyond the Zenneck stage, as could have been predicted solely on the basis of a comparison of the relative magnitudes of ε_x' and ε_x''. At room temperature ε_x'' is greater than $|\varepsilon_x'|$ in the frequency range where ε_x' is negative.

Theoretical calculations of the characteristics of ESP's on the (010) face of TCNQ° suggest them to be more complex. Experimentally we find that at the low frequency edge of the stop-band the ESP looks like a damped Brewster mode since almost all the ATR minima lie in the radiative region. However, since $\varepsilon_x' < 0$ it can also be described as a Zenneck mode. This is an interesting point, namely just because ε_x' is negative the ATR minimum need not occur in the nonradiative region. In the presence of strong absorption and a suitable ε_z the surface mode may give rise to a minimum in the radiative region. Accordingly in this situation one does not need prism to detect the minimum in reflection due to the surface mode. However, actual calculations show that in the absence of a coupling prism the minimum is extremely broad and would be very difficult to detect experimentally. At higher frequencies, near the upper edge of the stop-band of TCNQ°, there is a range of negative ε_x' where $|\varepsilon_x'| \gg \varepsilon_x''$. In this range theoretical calculation of the ATR minimum show them to lie several degrees past the light line, and in this case the ESP may be truly described as a Zenneck or very lossy Fano mode.

The following conclusions can be drawn concerning virtual ESP's on organic crystal surfaces at room temperature. First of all the ESP's are likely to be heavily damped throughout the stop-band and therefore to behave mainly as Zenneck modes. Second, in materials with very wide polariton stop-bands there may be several regions of Zenneck and lossy Fano behavior because of fluctuations in the magnitudes of ε_x' and ε_x'' due to vibronic transitions. At room temperature the existence of high molecular symmetry, like D_{2h} in the case of TCNQ°, is not likely to give rise to any qualitatively new features in the ATR spectra because thermal broadening more than counteracts the sparseness of totally symmetric vibrational modes. This will not apply at low temperatures, however.

It is clear from this work that ESP's should be observable at room temperature on many if not all the organic "metallic reflectors." The sensitivity of surface polaritons to the physical condition of the surface is well established from work with plasmon and phonon surface polaritons. It seems possible that exciton surface polaritons could be used as sensitive probes of the surface layers of the highly reflecting organic solids. This may prove to be useful for organics since many of the surface science tools available for studying inorganic materials, cannot be used for studying organic surfaces; for example, they are notoriously sensitive to damage by electron beams.

It is the "resonance" enhancement of the electromagnetic field at the crystal surface that makes ESP's sensitive to the conditions at the surface. Calculation can model changes at a surface by the insertion of a boundary layer of varying optical properties. This is well known from theoretical and experimental work on inorganic solids. The importance for organic solids like PTS is that we can, in principle, use this technique to study the effects of

adsorbed layers on a "clean" crystal surface. ATR spectroscopy has also the potential for studying chemical reactions with very small quantities of reagent on highly reflecting solids like PTS. Another possibility is for comparative studies of different crystal faces, such as (100) and (102), which both contain the *b* component of the crystal transition. Physically these two surfaces are expected to behave differently since contraction during polymerization affects the (102) face more than the (100) face.

Another logical extension is to lower temperatures where the damping is smaller, and where the possibility exists of observing the interaction of the surface polariton with the vibronic states of the surface region. The case of anthracene is of particular interest because of the existence of site shift surface exciton. Model calculations indicate that the ESP will couple very strongly to these other two dimensional states. A hint of this interaction can be found in the experimental study of Tomioka, *et al.*[7]

There are numerous experiments that can be done at room temperature, too. A few of the more obvious ones are: (i) use of the enhanced electromagnetic field intensity to perform resonance Raman and fluorescence excitation experiments, (ii) nonlinear processes involving polariton fusion, or the population of photoconduction states, (iii) dephasing experiments.

In summary the existence of exciton polariton states on the surfaces of molecular crystals has been shown to be phenomenon that is not only easier to detect than was heretofore suspected but also has some promise in providing information of the physical condition of surfaces.

Acknowledgments

We are indebted to R. Santo for technical assistance, E. Nazzal for synthesizing the dye CTIP, T. C. Clarke for synthesizing 2,4-hexadiyne-1,6-diol bis(p-toluene sulphonate), D. Miller for providing the TCNQ° crystals, and E. Kretschmann for suggesting the use of a focused light beam.

References

1. B. G. Anex and W. T. Simpson, *Rev. Mod. Phys.*, **32**, 466 (1960).
2. J. Lagois and B. Fischer, *Phys. Rev. Letters*, **36**, 680 (1976); *Solid State Communications*, **18**, 1519 (1976).
3. I. Hirabayashi, T. Koda, Y. Tokura, J. Murata and Y. Kaneko, *J. Phys. Soc. Jap.*, **40**, 1215 (1976).
4. I. Hirabayashi, T. Koda, Y. Tokura, J. Murata and Y. Kaneko, *J. Phys. Soc. Jap.*, **43**, 173 (1977).
5. Y. Tokura, I. Hirabayashi and T. Koda, *J. Phys. Soc. Jap.*, **42**, 1071 (1977).
6. T. Koda, personal communication.
7. K. Tomioka, M. G. Sceats and S. A. Rice, *J. Chem. Phys.*, **66**, 2984 (1977).
8. I. Pockrand, A. Brillante, M. R. Philpott and J. D. Swalen *Opt. Comm.*, **27**, 91 (1978).
9. A Brillante, I. Pockrand, M. R. Philpott and J. D. Swalen, *Chem. Phys. Letters* **57**, 395 (1978).

10. There are several review articles that give references to the early work as well as describing recent experimental and theoretical work on surface polaritons, for example: (a) A. Otto, "Experimental Investigation of Surface Polaritons on Plane Interfaces," *Advances in Solid State Physics/Festkorperprobleme*, **14**, 1–37 (1974); (b) G. Borstel, H. J. Falge and A. Otto, "Surface and Bulk Phonon Polaritons Observed by Attentuated Total Reflection," Springer Tracts in Modern Physics, *Solid State Physics*, **74**, 107–148 (1974); (c) H. Raether, "Surface Plasma Oscillations and Their Applications," *Physics of Thin Films* (Academic Press, New York) **9**, 145–261 (1977); (d) A. Otto, "Spectroscopy of Surface Polaritons by Attenuated Total Reflection," in *Optical Properties of Solids, New Developments*, edited by B. O. Seraphin (North-Holland, New York, 1976), Chap. 13, pp. 677–727.
11. M. R. Philpott, *Phys. Rev.*, **B14**, 3471 (1976).
12. *Polaritons*. Proceedings of the First Taormina Conference on the Structure of Matter, edited by E. Burstein and F. DeMartini (Pergamon Press, New York, 1974).
13. A. Hartstein, E. Burstein, J. J. Brion and R. F. Wallis, *Surf. Science*, **34**, 81 (1973).
14. G. Borstel, *Phys. Status Solidi (b)*, **60**, 42 (1973).
15. A. Hartstein, E. Burstein, J. J. Brion and R. F. Wallis, *Polaritons*, see Reference 12, pp. 111–116.
16. E. Tosatti and G. Harbeke, *Nuovo Cim.*, **22B**, 87 (1974); D. L. Mills and E. Burstein, *Rep. Prog. Phys.*, **37**, 817 (1974).
17. W. T. Simpson and D. L. Peterson, *J. Chem. Phys.*, **26**, 588 (1957).
18. E. Kretschmann, *Opt. Comm.* **26**, 41 (1978).
19. C. R. Fincher, Jr., D. L. Peebles, A. J. Heeger, M. A. Druy, Y. Matsumura, A. G. MacDiarmid, H. Shirakawa and S. Ikeda, "Anisotropic Optical Properties of Pure and Doped Polyacetylene," *Solid State Comm.*, **27**, 489 (1978).
20. W. Bludau, T. C. Clarke, P. M. Grant and G. B. Street, "Optical Properties of Polyacetylene Before and After Doping," *Preprint*, 1978.
21. H. J. Hesse, W. Fuhs, G. Weiser and L. von. Szentpaly, *Chem. Phys. Letters*, **41**, 104 (1976).
22. H. J. Hesse, W. Fuhs, G. Weiser and L. von Szentpaly, *Phys. Status Solidi (b)*, **76**, 816 (1976).
23. R. Allman, T. Debaerdemaeker, A. R. Ferwanah, W. Pressler and C. Reichardt, *Chem. Berichte*, **109**, 3005 (1976).
24. D. Kobelt and E. F. Paulus, *Acta Crystallogr.*, **B30**, 232 (1974).
25. R. Reimer, H. Baessler, J. Hesse and G. Weiser, *Phys. Status Solidi (b)*, **73**, 709 (1976).
26. D. Bloor, D. J. Ando, F. H. Preston and C. G. Stevens, *Chem. Phys. Letters*, **24**, 407 (1974).
27. D. Bloor and F. H. Preston, *Phys. Status Solidi (a)*, **37**, 427 (1976).
28. H. Müller and C. J. Eckhardt, *J. Chem. Phys.*, **67**, 5386 (1977).
29. K. Syassen and M. R. Philpott, unpublished observations.
30. R. E. Long, R. A. Sparks and K. N. Trueblood, *Acta Crystallogr.*, **18**, 932 (1962).
31. R. R. Pennelly and C. J. Eckhardt, *Chem. Phys.*, **12**, 89 (1976).
32. M. R. Philpott, P. M. Grant, K. Syassen and J. M. Turlet, *J. Chem. Phys.*, **67**, 4229 (1977).
33. J. Lagois and B. Fischer, *Phys. Rev. B.*, **17**, 3814 (1978).